Key Engineering Materials
ISSN: 1662-9795, Vol. 926, pp 1223-1233
doi:10.4028/p-a51g25

Submitted: 2021-11-26
Revised: 2022-01-12
Accepted: 2022-02-18
Online: 2022-07-22

A Hypoelastic Approach for Simulating the Independent Bending Behavior of Textile Composite within the Stress Resultant Shell

Bo Chen[1,a*], Philippe Boisse[1,b], Julien Colmars[1,c], Naim Naouar[1,d]

[1]Université de Lyon, LaMCoS, CNRS, INSA-Lyon, F-69621, France

[a]bo.chen@insa-lyon.fr, [b]philippe.boisse@insa-lyon.fr, [c]julien.colmars@insa-lyon.fr, [d]naim.naouar@insa-lyon.fr

*Corresponding author

Keywords: Drape simulation, Hypoelastic, Stress resultant shell, Textile composite.

Abstract: In the textile composite drape process, the material bending behavior plays a critical role in the onset and development of wrinkles. The bending moment is linked with the membrane force in the classical shell element which leads to the insufficient for the textile composite draping simulation. Specific to the textile composite, a hypoelastic approach is proposed within the stress resultant shell. A bending stiffness independent of membrane stiffness is introduced to calculate the stress moments in the finite element analysis. This approach is implemented in the commercial software Abaqus, which makes it possible for any user of this software.

1. Introduction

Numerical simulation of the textile composites forming has become a hot topic in the past several decades [1-3]. The textile composites are not continuous at the microscale and mesoscale, but it can be seen as a continuous medium on average at the macroscopic scale in the simulation model [2, 4]. Modeling the textile composite at macroscale will decrease the number of the finite element, and the wrinkles can be observed at the macroscale simulation model which is one of the main forming defects [5-7].

For a single layer of textile composites, the dimension in the thickness direction is much smaller than the other two directions, shell finite element modeling is much more efficient than 3D finite element modeling. Some research works were devoted to shell formulation development. Based on the quasi-inextensibility of fiber, Liang et al. and Renzi et al. [8, 9] developed a fibrous shell focusing on the shear deformation in the thickness direction. The textile material behavior highly depends on the yarn direction, Peng et al [10] developed a non-orthogonal constitutive model to update material behavior law on the changing yarn directions. Khan et al. and Bo et al. [11, 12] implemented a hypoelastic model using an objective derivative defined from the yarn rotation. The textile composite bending stiffness is much smaller than the value given by the classical shell theory. To consider this bending behavior independent of the membrane behavior, a hypoelastic model in the stress resultant shell is introduced based on the fiber physics deformation mechanism in this article.

2. The Bending Behavior of the Textile Composite

The textile composite material is weaved by two initial perpendicular yarns (called warp and weft yarns). Due to the possible relative slippage between warp and weft yarns, the material bending stiffness is much lower than the bending stiffness calculated from the classical theory for a given membrane stiffness.

The difference of the bending deformation between the textile composite and classical continuous material is given in Fig. 1, Fig. 1a shows the three-point bending of a classical continuous material (15mm thick silica gel), and Fig. 1b shows the three-point bending of the textile composite (15mm thick interlock fabric [13]). In the bending deformation, the middle surface and the material director which is initially perpendicular to the middle surface are both marked in the two materials. The material directors remain perpendicular to the middle surface in the classical continuous material (Fig.

1a) which is following Kirchhoff's theory. This is not the same as the bending of textile composite. And it can be seen that the material directors do not keep perpendicular to the middle surface when the material deformed, which is due to the material quasi-inextensibility in the yarn direction and the slippage between yarns.

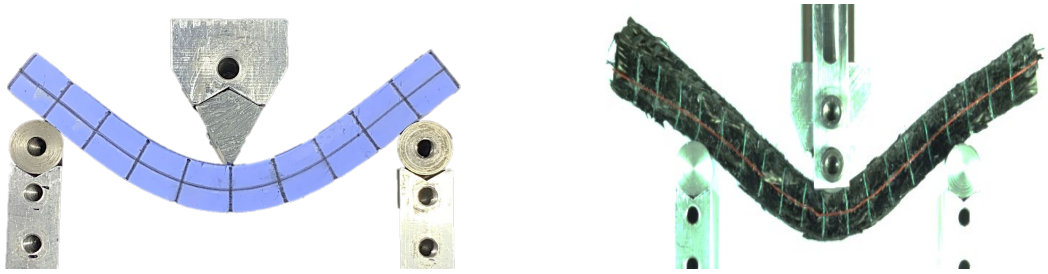

(a) (b)

Fig. 1. (a) Bending of a classical continous material (b) Bending of a fibous material

For the classical continuous material following Kirchhoff's assumption, the bending stiffness can be directly obtained as followed:

$$B_{\text{classic}} = \frac{Eh^3}{12(1-\nu^2)} \tag{1}$$

Here E is the Young's modulus, h is the material thickness and ν is the material Poisson ratio. According to the bending experiment comparison shown in Fig. 1, it can be known that Eq. 1 cannot be used to calculate the bending stiffness of textile material. The bending behavior of the textile material is independent of the membrane behavior.

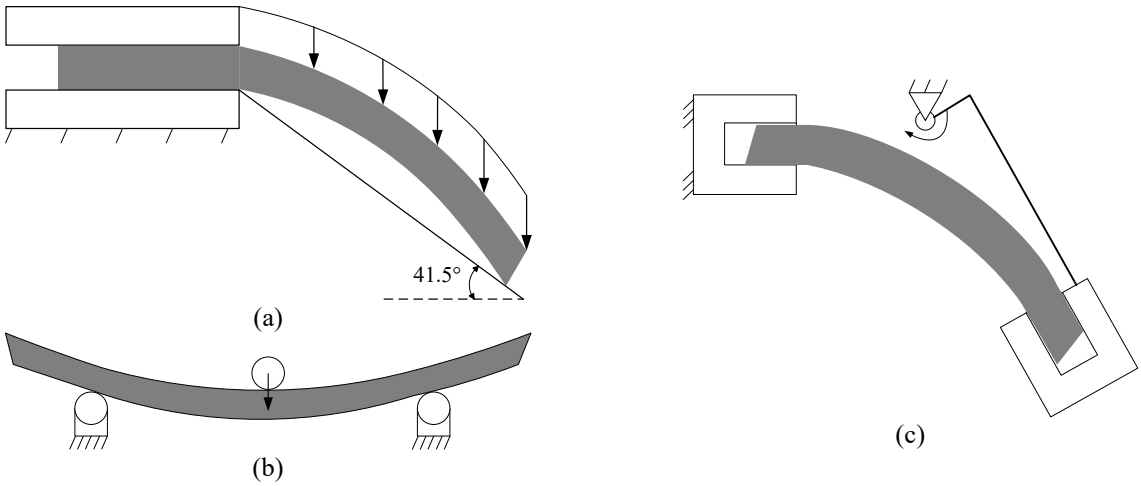

Fig. 2. Schematic diagram to test the bending stiffness (a) Pierce bending test (b) Three point bending test (c) Kawabata bending test (KES-FB2)

In order to research the bending behavior of the textile material, several methods have been proposed in the literature to measure the bending stiffness (shown in Fig. 2). Fig. 2a is the Pierce bending test [14], this test is based on the cantilever bending of a specimen subjected to its own gravity. An inclined plane at 41.5° is placed in the experiment. The material bending stiffness is assumed as linear. When the bending of the tested material reaches the inclined plane, the material bending stiffness can be obtained by measuring the bending length [15]. Fig. 2b is the three-point bending test [16], this test can be used to test thick enough textile composites or the material with small thickness. The curvature of the material is obtained by the image processing, and the moment applied to the specimen is recorded by the load sensor. Then the relationship of bending moment with curvature can be determined by post-processing. Fig. 2c is the Kawabata bending test (KES-FB2) [17], the specimen is bent into a constant curvature by the rotation of one clamp, and the bending moment is obtained directly by the device. This approach can be used to research the relationship of the bending rate with the bending stiffness [18, 19].

The bending stiffness is rather low compared with the material membrane behavior. However, some previous research had found that bending stiffness play an important role in the onset and development of the possible wrinkles when the material deformed into the desired geometry [7, 15, 20-22]. In order to correctly predict the material deformation in the draping simulations, several simulation models have been proposed considering the independent bending behavior. The first approach shown in Fig. 3a considers a single layer of textile composite as laminated shells with different Young moduli and thickness, the membrane and bending behavior of a single-layer material are obtained by designing the characteristics of the laminated shells [20]. Another method (shown in Fig. 3b and c) is to model the bending behavior independent of the membrane behavior through the superimposition of different finite elements. Fig. 3b combines the beam elements (to model bending behavior) in the warp and weft yarn direction with membrane element (to model membrane behavior) [23]. Fig. 3c is the superposition of membrane element and shell element. The membrane behavior is simulated by the membrane element and the small bending stiffness is obtained by setting a relatively small Young modulus in the shell element.

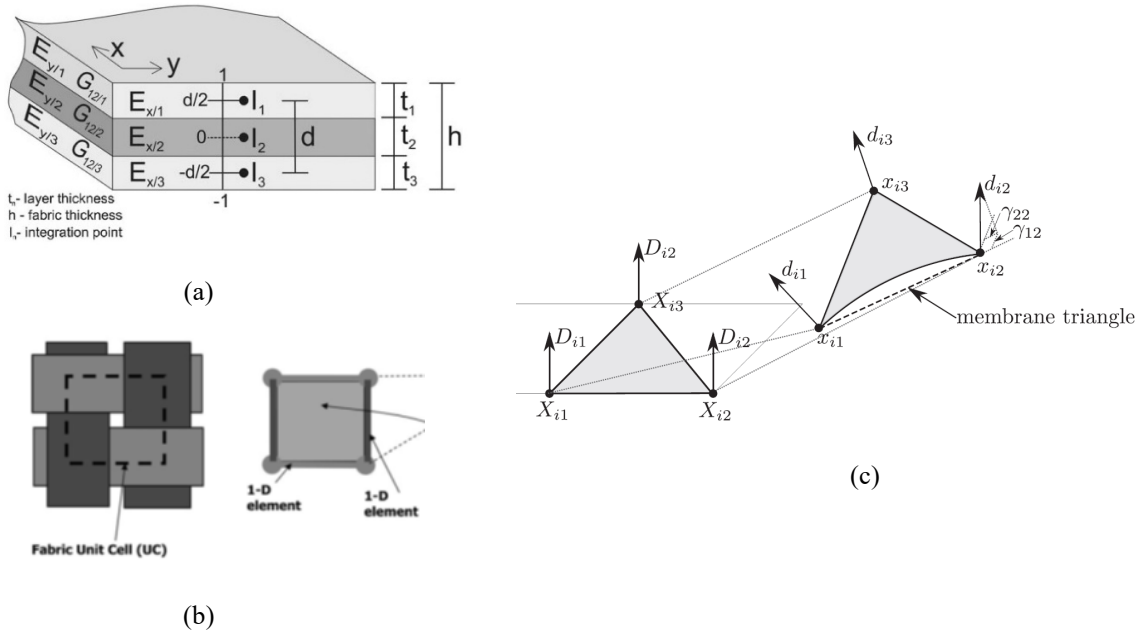

Fig. 3. Different approaches to simulate the independent bending behavior. (a) Laminated approach [20]. (b)Modeling by beam and membrane element [23]. (c) Superposition of a membrane and shell element [24].

These approaches presented in Fig. 3 give a solution to consider the independent bending behavior in the simulation. They are effective in predicting the middle surface deformation of the textile composite at the macroscale. However, these approaches are somewhat artificial and neglect the physics mechanism of the fibrous material bending. To overcome this shortcoming, a hypoelastic approach is presented and introduced below. The bending and membrane behavior are considered independently within a stress resultant shell element. This approach can be implemented in the commercial software Abaqus subroutine VUGENS which can be available by any user of Abaqus.

3. The Hypoelastic Approach in the Stress Resultant Shell

For any virtual displacement equal to zero on the imposed displacement boundary part, the virtual work equation links internal virtual work δW_{int}, external virtual work δW_{ext} and acceleration virtual work δW_{acc}:

$$\delta W_{\text{ext}} - \delta W_{\text{int}} = \delta W_{\text{acc}} \tag{2}$$

In the stress resultant shell element, the internal virtual work can be calculated as:

$$\delta W_{\text{int}} = \int_A (\delta\varepsilon_{11} N_{11} + \delta\varepsilon_{22} N_{22} + \delta\varepsilon_{12} N_{22} + \delta\chi_{11} M_{11} + \delta\chi_{22} M_{22} + \delta\chi_{12} M_{12}) dA \tag{3}$$

Here A is the shell middle surface, $\delta\varepsilon_{11}$, $\delta\varepsilon_{22}$ are the virtual axial strains in the warp and weft directions, $\delta\varepsilon_{12}$ is the virtual in-plane shear strain, $\delta\chi_{11}$, $\delta\chi_{22}$, $\delta\chi_{12}$ are the virtual curvatures in these directions. N_{11}, N_{22}, N_{12} are the stress resultants and M_{11}, M_{22}, M_{12} are the stress moments (or couples) with the expression:

$$N_{\alpha\beta} = \int_{-\frac{h}{2}}^{\frac{h}{2}} \sigma_{\alpha\beta} dz \qquad M_{\alpha\beta} = \int_{-\frac{h}{2}}^{\frac{h}{2}} z\sigma_{\alpha\beta} dz \tag{4}$$

In this article, the Greek indices α, β will belong to the set (1,2). The stress resultants and moments in a unit woven element is presented in Fig. 4. (M_{12} is neglected which assumes that the bending stiffness of the textile composite is given by the two yarns. In the other aspects, this is aso because of the difficulty in the measuring the cross bending stiffness.)

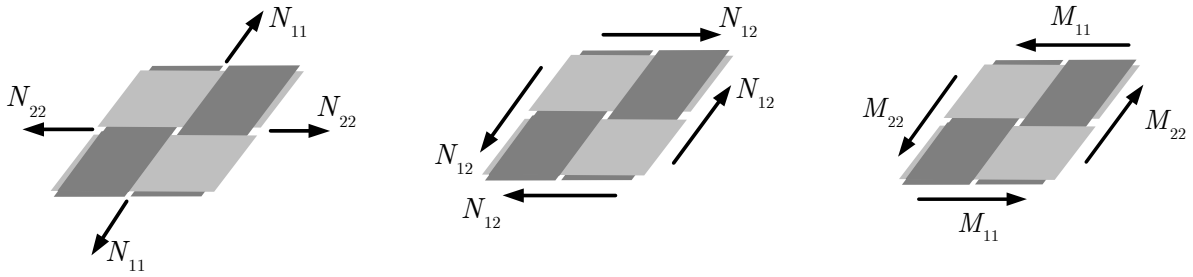

(a) (b) (c)

Fig. 4. The stress resultants and moment in a unit woven element. (a) Tensile (b) In plane shear (c) Bending

According to Eq. 4, the stress moments $M_{\alpha\beta}$ are obtained through the intergration of the Cauchy streess $\sigma^{\alpha\beta}$ over the thickness of the shell element. Thus for the conventional analyses in the shell elelment, the bending behavior is coupled with the membrane behavior. According to the previous discussion, this is not the case for the textile compsite material. In oder to simulate the independent bending behavior in the stress resulant shell element, a hypoelastic behavior is adopted as below:

$$\mathbf{N}^{\nabla} = \mathbf{C} : \dot{\varepsilon} \qquad \mathbf{M}^{\nabla} = \mathbf{D} : \dot{\chi} \tag{5}$$

Here, $\dot{\varepsilon}$ and $\dot{\chi}$ are the time derivatives of the membrane strain $\varepsilon_{\alpha\beta}$ and curvature tensors $\chi_{\alpha\beta}$, $\mathbf{C}$ and $\mathbf{D}$ are the membrane and bending constitutive tensors, $\mathbf{N}^{\nabla}$ and $\mathbf{M}^{\nabla}$ are the objective derivatives of the stress resultant $N_{\alpha\beta}$ and stress moment $M_{\alpha\beta}$. The objective derivative is the time derivative for an observer fixed to the material. The aim is that no stress is created by the rigid body rotations.

Following the Eq. 5, the resultant stress $N_{\alpha\beta}$ will be related to the membrane strains $\varepsilon_{\alpha\beta}$, and the resulant memonts $M_{\alpha\beta}$ will be related to the curvature $\chi_{\alpha\beta}$. The calculation of the stress resultant and stress moment will be independent. Thus the bending behavior will be naturally independent of the membrane behavior which is for the textile composite material.

For the rotational objective derivatives, the most classical rotation derivatives are those of Jaumann [25] and of Green Naghdi [26]. In the textile composite, the material behavior highly depend on the yarn direction. In the Abaqus/explicit subroutine, the Green Naghdi derivatives are adopted, and the input and output quantities are expressed in the Green Naghdi frames (Obtained by polar decomposition of deformation gradient tensor *F*). The approach presented below will introduce the implantation of the textile composite constitutive equation in the Green Naghdi frame.

As shown in Fig. 5, the two yarn directions $(\mathbf{f}_1^0, \mathbf{f}_2^0)$ usually don't remain orthogonal when the textiles deformed because of the shear deformation. They can be calculated by the deformation gradient tensor *F*.

$$\mathbf{f}_{\alpha} = \frac{\mathbf{F} \cdot \mathbf{f}_{\alpha}^{\mathbf{0}}}{\left\| \mathbf{F} \cdot \mathbf{f}_{\alpha}^{\mathbf{0}} \right\|} = \frac{\mathbf{F} \cdot \mathbf{e}_{\alpha}^{\mathbf{0}}}{\left\| \mathbf{F} \cdot \mathbf{e}_{\alpha}^{\mathbf{0}} \right\|} \tag{6}$$

Two independent orthogonal fiber frames are constructed: one basis directed by the warp fiber direction $\mathrm{g}(\mathbf{g}_1, \mathbf{g}_2)$ with $\mathbf{g}_1 = \mathbf{f}_1$ and the other directed by the weft fiber direction $\mathrm{h}(\mathbf{h}_1, \mathbf{h}_2)$ with $\mathbf{h}_2 = \mathbf{f}_2$

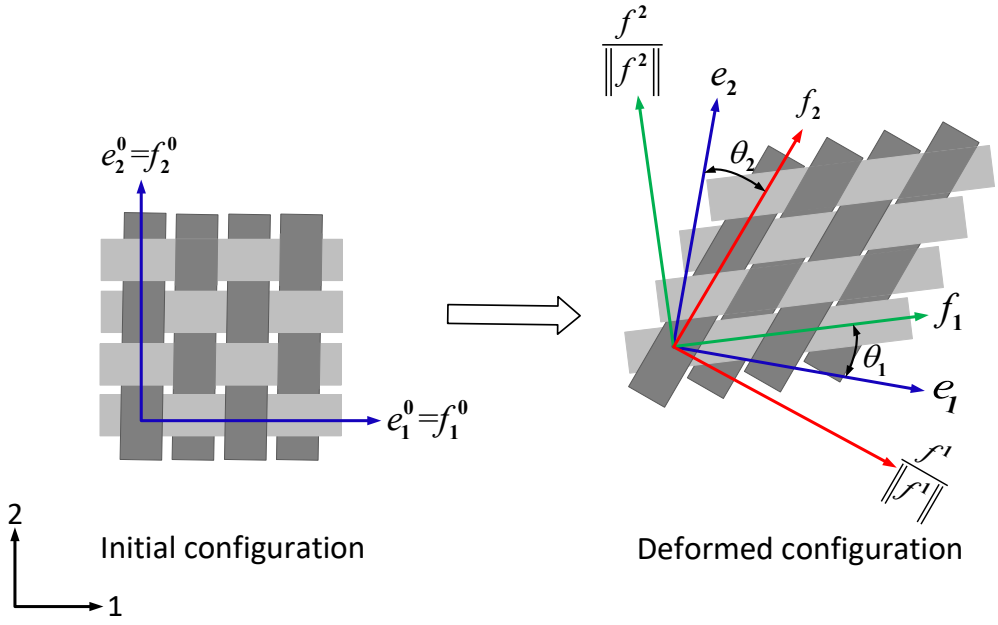

Fig. 5. The constructed fiber frames and the Green-Naghdi frames

For the time increment $[t_n, t_{n+1}]$, the components of the membrane deformation increment and the curvature increment are given on the Green Naghdi basis:

$$\mathbf{d\varepsilon} = d\varepsilon_{\alpha\beta}^{GN}\mathbf{e}_\alpha \otimes \mathbf{e}_\beta \qquad \mathbf{d\chi} = d\chi_{\alpha\beta}^{GN}\mathbf{e}_\alpha \otimes \mathbf{e}_\beta \tag{7}$$

Through tensor transformation, the components of the membrane and curvature tensors on the bases of g and h can be deduced from:

$$\begin{aligned} [d\varepsilon]_g &= [T_1]^T\,\mathbf{d\varepsilon}[T_1] \quad [d\varepsilon]_h = [T_2]^T\,\mathbf{d\varepsilon}[T_2] \\ [d\chi]_g &= [T_1]^T\,\mathbf{d\chi}[T_1] \quad [d\chi]_h = [T_2]^T\,\mathbf{d\chi}[T_2] \end{aligned} \tag{8}$$

Here, $[T_\alpha]$ are the transform matrix between the Green Naghdi frame and the two fiber frames g, h.

According to these obtained increments of membrane and curvatures tensors, the material constitutive equation will be used here to calculate the components of the stress resultant and stress moment on the bases of g and h.

$$\begin{aligned} [dN]_g &= [C]_g[d\varepsilon]_g \qquad [dN]_h = [C]_h[d\varepsilon]_h \\ [dM]_g &= [D]_g[d\chi]_g \qquad [dM]_h = [D]_h[d\chi]_h \end{aligned} \tag{9}$$

Three material behaviors at the macroscale (tensile stiffness, in-plane shear stiffness and out-of-plane bending stiffness) are considered here, which play a main role in the material deformation. Then the Eq. 9 can be explicitly written as:

$$\begin{bmatrix} dN_{11} \\ dN_{22} \\ dN_{12} \end{bmatrix}_g = \begin{bmatrix} C_{11} & 0 & 0 \\ 0 & 0 & 0 \\ 0 & 0 & C_{12} \end{bmatrix}_g \begin{bmatrix} d\varepsilon_{11} \\ d\varepsilon_{22} \\ d\varepsilon_{12} \end{bmatrix}_g \quad \begin{bmatrix} dN_{11} \\ dN_{22} \\ dN_{12} \end{bmatrix}_h = \begin{bmatrix} 0 & 0 & 0 \\ 0 & C_{22} & 0 \\ 0 & 0 & C_{12} \end{bmatrix}_h \begin{bmatrix} d\varepsilon_{11} \\ d\varepsilon_{22} \\ d\varepsilon_{12} \end{bmatrix}_h$$
$$\begin{bmatrix} dM_{11} \\ dM_{22} \\ dM_{12} \end{bmatrix}_g = \begin{bmatrix} D_{11} & 0 & 0 \\ 0 & 0 & 0 \\ 0 & 0 & D_{12} \end{bmatrix}_g \begin{bmatrix} d\chi_{11} \\ d\chi_{22} \\ d\chi_{12} \end{bmatrix}_g \quad \begin{bmatrix} dM_{11} \\ dM_{22} \\ dM_{12} \end{bmatrix}_h = \begin{bmatrix} 0 & 0 & 0 \\ 0 & D_{22} & 0 \\ 0 & 0 & D_{12} \end{bmatrix}_h \begin{bmatrix} d\chi_{11} \\ d\chi_{22} \\ d\chi_{12} \end{bmatrix}_h \tag{10}$$

Here, C_{11}, C_{22} are the tensile stiffness in the warp and weft directions respectively, C_{12} is the in-plane shear stiffness, D_{11}, D_{22} are the out-of-plane bending stiffness in the warp and weft directions and D_{12} it is the cross term of bending stiffness (D_{12} is set as zero in the constitutive equations). These stiffnesses are not necessarily constant, they can be linear or non-linear, especially C_{12} depends on the in-plane shear which is experimental measured as non-linear for textile composites.

In the simulation step time $[t_n, t_{n+1}]$, the stress resultants and stress moments are cumulated following the Hughes and Winget scheme [27]:

$$[N]_g^{n+1} = [N]_g^n + [dN]_g^{n+1/2} \quad [N]_h^{n+1} = [N]_h^n + [dN]_h^{n+1/2}$$
$$[M]_g^{n+1} = [M]_g^n + [dM]_g^{n+1/2} \quad [M]_h^{n+1} = [M]_h^n + [dM]_h^{n+1/2} \tag{11}$$

Then the stress resultants and stress moment on the Green Naghdi base e can be obtained by adding those quantities in the basis g and h after transformation: (n+1 index is omitted, all the quantities are at t_{n+1})

$$[N]_e = [T_1][N]_g[T_1]^T + [T_2][N]_h[T_2]^T$$
$$[M]_e = [T_1][M]_g[T_1]^T + [T_2][M]_h[T_2]^T \tag{12}$$

4. Bending Behavior Verification

The cantilever bending experiment and the corresponding simulation are conducted to verify the presented approach. The material Hexcel G1151 (shown in Fig. 6) is chosen for the cantilever bending experiment. In the experiment, a single layer of G1151 is bent under its gravity. This experiment is an extension of the Pierce bending test (Fig. 2a) to test the material bending stiffness [28]. The deformed midline of the specimen is obtained by the imaging process, and the bending moment at different positions on the midline is determined by the weight of the specimen. Thus the bending stiffness of the specimen can be obtained by taking derivate of the moment-curvature.

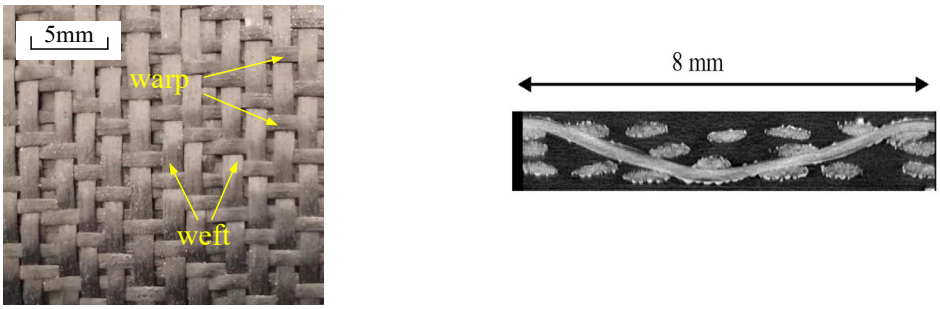

Fig. 6. Hexcel G1151 architecture

The bending stiffness along the warp and weft yarn of the Hexcel G1151 are all tested using this method [29, 30] , the bending section shapes given by the experiment are shown in Fig. 7a and c. The tested bending stiffness along the two direction yarns are:

$$D_{11} = 10.5 \text{ N mm} \quad D_{22} = 4.3 \text{ N mm} \tag{13}$$

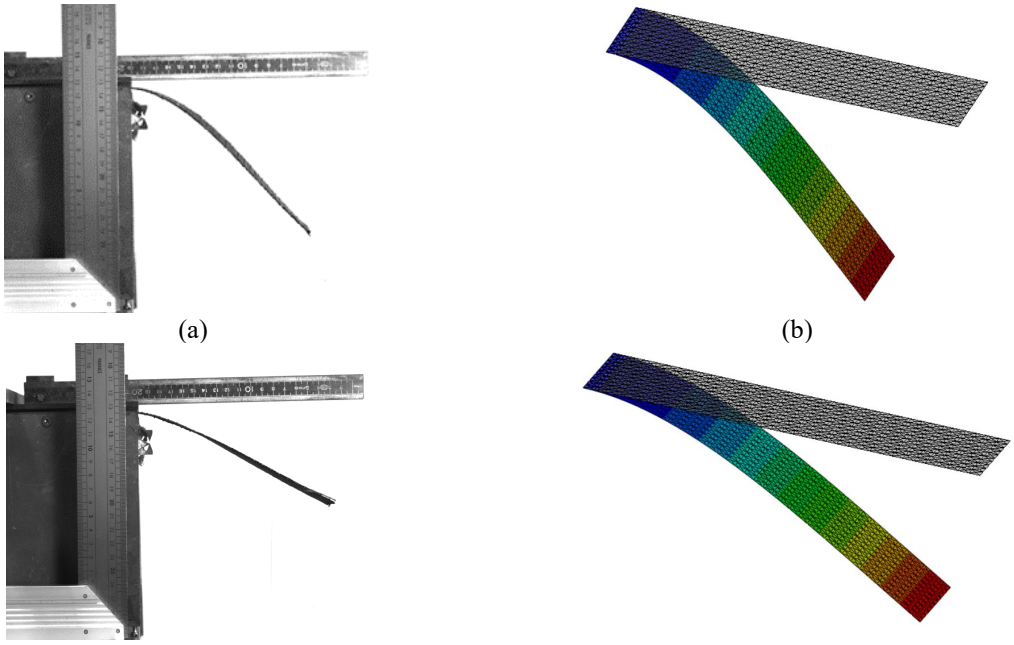

(a) (b) (c) (d)

Fig. 7. Cantilever test of G1151 interlock fabric. (a) Bending experiment alone warp yarn (b) Bending simulation alone warp yarn (c) Bending experiment alone weft yarn (d) Bending simulation alone weft yarn

Then the bending simulation using the presented approach is conducted to make comparison with the experiment. In the simulation, the tensile stiffness of the yarn in the two directions are set as $C_{11} = C_{22} = 10000$ N mm^{-1} which can be seen as quasi-inextensibility in the yarn direction, and the bending stiffness is from the bending experiment result (Eq. 13). The 3-node shell element is selected for the numerical analysis. The simulations result of the bending section in the warp and weft yarns directions are presented in Fig. 7b and d respectively. The bending sections shape are also extracted to make the comparison (Fig. 8). It can be found that the bending results are in good agreement between the experiment and simulation.

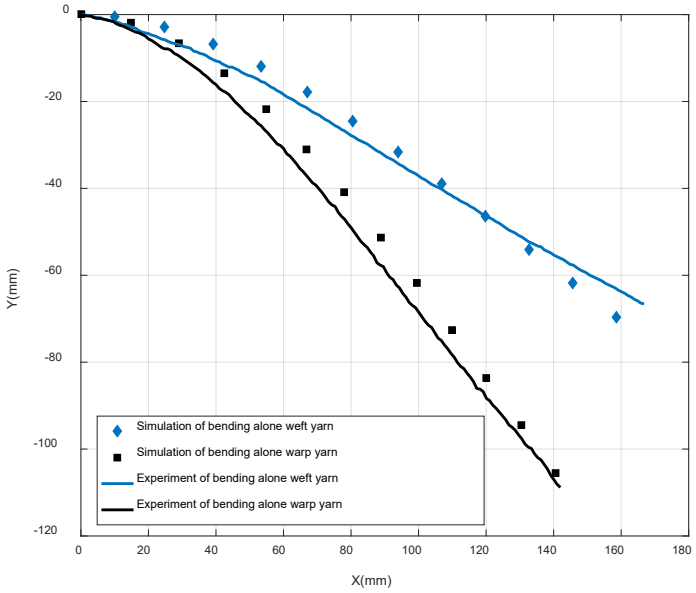

Fig. 8. Simulation and experiment results of bending section shape.

5. Multi-Layers Hemisphere Forming

To study the capabilities of the presented approach in the textile composite forming, the forming experiment and corresponding are done on a stack of several plies. In the simulation process, each

ply of the textile composite is modeled independently (Shown in Fig. 9). The contact property is applied between adjacent layers, with a Coulomb friction coefficient of 0.2.

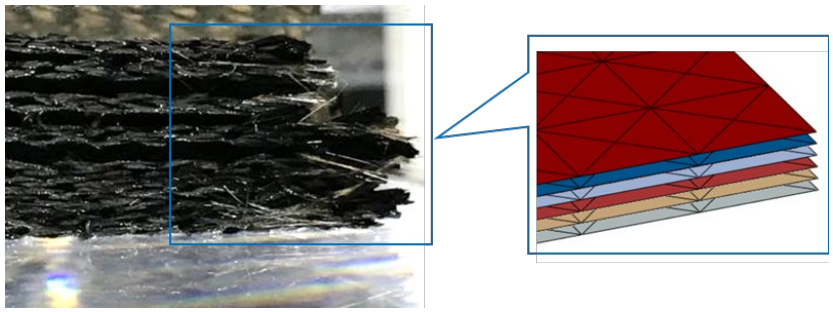

Fig. 9. Simulation modelling for the multi-layers forming

The material used in the experiment is the Hexcel G1151, the thickness of a single ply is 1.3 mm. The tensile stiffness and bending stiffness are given in section 4. For the in-plane shear stiffness, it can be determined by the bias-extension test or picture frame [31, 32]. The bias extension test of G1151 is conducted and the in-plane shear stiffness is:

$$C_{12} = 0.088 - 0.83|\gamma| + 2.92|\gamma|^2 - 4.01|\gamma|^2 + 2.03|\gamma|^4 \ (\gamma = 2\varepsilon_{12}) \tag{14}$$

Here γ is the in-plane shear angle.

In the forming experiment, the blank holder and die module were made transparent to observe the material deformation during the forming process. Two cameras were placed at the material top side and bottom side respectively, through the reflection of the mirror, pictures were recorded with image software. The forming geometry parameters are presented in Fig. 10. When preparing the material, maker points are drawn on the surface, the marker-based tracking approach is adopted to get the material deformation in the different locations. Four layers with quasi-isotropic layer-up are adopted in the experiment and the material initial dimension is 300 mm × 300 mm. The final punch displacement in the forming is 75 mm.

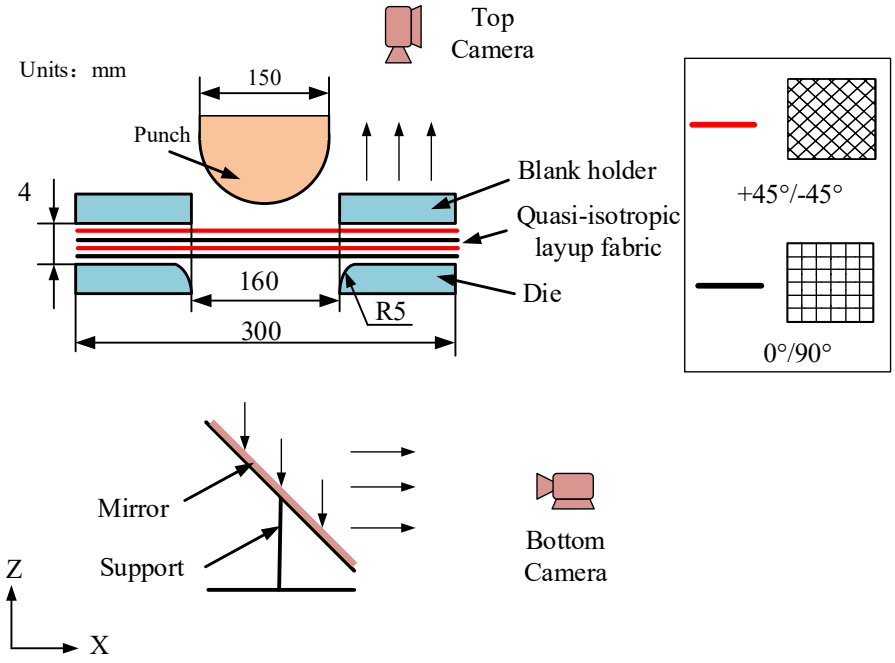

Fig. 10. The set-up of hemisphere forming

The final deformed material shapes are presented on the lefthand of Fig. 11, including the top view and bottom view. The corresponding simulation results using the presented approach are given in the righthand of Fig. 11. The shear angle at the different zone is compared between simulation and experiment. The shear angle results of the experiment are obtained with the help of the marker points.

As it can be seen in Fig. 11, the final deformed shape and the shear angle in the different zone are in good agreement between simulation and experiment.

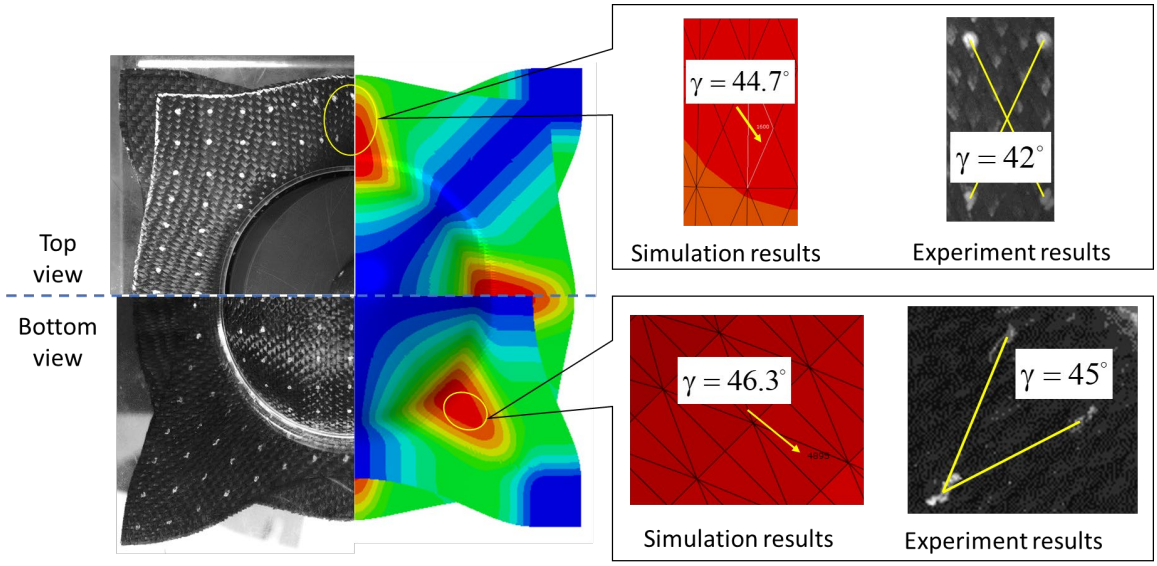

Fig. 11. Comparision of the simulation results with experiment

6. Conclusion

The textile composites are composed of thousands of fibers in small diameters, which gives very specific mechanical properties. The material bending stiffness is smaller than the value given by the classical shell theory based on the Kirchhoff assumption. In the conventional analyses in the shell element, the bending moment is calculated through the integration of the Cauchy stress, which leads to the coupling between the shell bending behavior and the membrane behavior. In order to conduct the textile composite forming simulation considering the independent bending behavior, a hypoelastic approach is proposed within the stress resultant shell element. The stress resultant is related to the membrane strain, and the stress moment is related to the bending curvature through the bending behavior independent of the membrane behavior. Through a set of comparisons between experiment and simulation, it is found that the presented approach is accurate and robust. The approach is implemented in the commercial software Abaqus, which makes it possible to conduct the textile composite forming for any user of Abaqus.

Acknowledgement

This work was supported by the ANR, (French Research Agency), grant ANR-18-CE06-0011-04-AMOC and by the China Scholarship Council (CSC) (B. Chen).

References

[1] Boisse, P.: Finite element analysis of composite forming. In: Composites Forming Technologies: A volume in Woodhead Publishing Series in Textiles. pp. 46–79. Elsevier Ltd (2007)

[2] Gereke, T., Döbrich, O., Hübner, M., Cherif, C.: Experimental and computational composite textile reinforcement forming: A review, (2013)

[3] Bussetta, P., Correia, N.: Numerical forming of continuous fibre reinforced composite material: A review, (2018)

[4] Boisse, P., Hamila, N., Madeo, A.: The difficulties in modeling the mechanical behavior of textile composite reinforcements with standard continuum mechanics of Cauchy. Some possible remedies. Int. J. Solids Struct. 154, 55–65 (2018). https://doi.org/10.1016/j.ijsolstr.2016.12.019

[5] Skordos, A.A., Monroy Aceves, C., Sutcliffe, M.P.F.: A simplified rate dependent model of forming and wrinkling of pre-impregnated woven composites. Compos. Part A Appl. Sci. Manuf. 38, 1318–1330 (2007). https://doi.org/10.1016/j.compositesa.2006.11.005
[6] Potter, K., Khan, B., Wisnom, M., Bell, T., Stevens, J.: Variability, fibre waviness and misalignment in the determination of the properties of composite materials and structures. Compos. Part A Appl. Sci. Manuf. 39, 1343–1354 (2008). https://doi.org/10.1016/j.compositesa.2008.04.016
[7] Boisse, P., Hamila, N., Vidal-Sallé, E., Dumont, F.: Simulation of wrinkling during textile composite reinforcement forming. Influence of tensile, in-plane shear and bending stiffnesses. Compos. Sci. Technol. 71, 683–692 (2011). https://doi.org/10.1016/J.COMPSCITECH.2011.01.011
[8] Liang, B., Colmars, J., Boisse, P.: A shell formulation for fibrous reinforcement forming simulations. Compos. Part A Appl. Sci. Manuf. 100, 81–96 (2017). https://doi.org/10.1016/j.compositesa.2017.04.024
[9] Bai, R., Colmars, J., Naouar, N., Boisse, P.: A specific 3D shell approach for textile composite reinforcements under large deformation. Compos. Part A Appl. Sci. Manuf. 139, 106135 (2020). https://doi.org/10.1016/j.compositesa.2020.106135
[10] Peng, X.Q., Cao, J.: A continuum mechanics-based non-orthogonal constitutive model for woven composite fabrics. Compos. Part A Appl. Sci. Manuf. 36, 859–874 (2005). https://doi.org/10.1016/j.compositesa.2004.08.008
[11] Khan, M.A., Mabrouki, T., Vidal-Sallé, E., Boisse, P.: Numerical and experimental analyses of woven composite reinforcement forming using a hypoelastic behaviour. Application to the double dome benchmark. J. Mater. Process. Technol. 210, 378–388 (2010). https://doi.org/10.1016/j.jmatprotec.2009.09.027
[12] Chen, B., Colmars, J., Naouar, N., Boisse, P.: A hypoelastic stress resultant shell approach for simulations of textile composite reinforcement forming. Compos. Part A Appl. Sci. Manuf. 149, 106558 (2021). https://doi.org/10.1016/J.COMPOSITESA.2021.106558
[13] Mathieu, S., Hamila, N., Bouillon, F., Boisse, P.: Enhanced modeling of 3D composite preform deformations taking into account local fiber bending stiffness. Compos. Sci. Technol. 117, 322–333 (2015). https://doi.org/10.1016/j.compscitech.2015.07.005
[14] Peirce, F.T.: 26—THE "HANDLE" OF CLOTH AS A MEASURABLE QUANTITY. J. Text. Inst. Trans. 21, T377–T416 (1930). https://doi.org/10.1080/19447023008661529
[15] Boisse, P., Colmars, J., Hamila, N., Naouar, N., Steer, Q.: Bending and wrinkling of composite fiber preforms and prepregs. A review and new developments in the draping simulations, (2018)
[16] Margossian, A., Bel, S., Hinterhoelzl, R.: Bending characterisation of a molten unidirectional carbon fibre reinforced thermoplastic composite using a Dynamic Mechanical Analysis system. Compos. Part A Appl. Sci. Manuf. 77, 154–163 (2015). https://doi.org/ https://doi.org/10.1016/j.compositesa.2015.06.015
[17] Kawabata, S.: The standardization and analysis of hand evaluation. (1980)
[18] Sachs, U., Akkerman, R.: Viscoelastic bending model for continuous fiber-reinforced thermoplastic composites in melt. Compos. Part A Appl. Sci. Manuf. 100, 333–341 (2017). https://doi.org/10.1016/j.compositesa.2017.05.032
[19] Pipes, R.B., Favaloro, A., Barocio, E., Hicks, J.: Pure bending of a continuous fiber array suspended in a thermoplastic polymer in the melt state. Compos. Part A Appl. Sci. Manuf. 149, 106561 (2021). https://doi.org/10.1016/J.COMPOSITESA.2021.106561
[20] Döbrich, O., Gereke, T., Diestel, O., Krzywinski, S., Cherif, C.: Decoupling the bending behavior and the membrane properties of finite shell elements for a correct description of the mechanical behavior of textiles with a laminate formulation. J. Ind. Text. 44, 70–84 (2013). https://doi.org/10.1177/1528083713477442
[21] Dangora, L.M., Mitchell, C.J., Sherwood, J.A.: Predictive model for the detection of out-of-plane defects formed during textile-composite manufacture. Compos. Part A Appl. Sci. Manuf. 78, 102–112 (2015). https://doi.org/10.1016/j.compositesa.2015.07.011

[22] Thompson, A.J., Belnoue, J.P.-H., Hallett, S.R.: Modelling defect formation in textiles during the double diaphragm forming process. Compos. Part B Eng. 202, 108357 (2020). https://doi.org/10.1016/j.compositesb.2020.108357
[23] Jauffrès, D., Sherwood, J.A., Morris, C.D., Chen, J.: Discrete mesoscopic modeling for the simulation of woven-fabric reinforcement forming. Int. J. Mater. Form. 3, 1205–1216 (2010). https://doi.org/10.1007/s12289-009-0646-y
[24] Dörr, D., Schirmaier, F.J., Henning, F., Kärger, L.: A viscoelastic approach for modeling bending behavior in finite element forming simulation of continuously fiber reinforced composites. Compos. Part A Appl. Sci. Manuf. 94, 113–123 (2017). https://doi.org/10.1016/j.compositesa.2016.11.027
[25] Dafalias, Y.F.: Corotational Rates for Kinematic Hardening at Large Plastic Deformations. J. Appl. Mech. 50, 561–565 (1983). https://doi.org/10.1115/1.3167091
[26] Dienes, J.K.: On the analysis of rotation and stress rate in deforming bodies. Acta Mech. 32, 217–232 (1979). https://doi.org/10.1007/BF01379008
[27] Hughes, T.J.R., Winget, J.: Finite rotation effects in numerical integration of rate constitutive equations arising in large-deformation analysis. Int. J. Numer. Methods Eng. 15, 1862–1867 (1980). https://doi.org/https://doi.org/10.1002/nme.1620151210
[28] Liang, B., Chaudet, P., Boisse, P.: Curvature determination in the bending test of continuous fibre reinforcements. Strain. 53, e12213 (2017). https://doi.org/ https://doi.org/10.1111/str.12213
[29] de Bilbao, E., Soulat, D., Hivet, G., Gasser, A.: Experimental Study of Bending Behaviour of Reinforcements. Exp. Mech. 50, 333–351 (2010). https://doi.org/10.1007/s11340-009-9234-9
[30] Chen, B., Boisse, P., Colmars, J., Naouar, N., Bai, R., Chaudet, P.: Analysis of the Forming of Interlock Textile Composites Using a Hypoelastic Approach. Appl. Compos. Mater. (2021). https://doi.org/10.1007/s10443-021-09966-z
[31] Cao, J., Akkerman, R., Boisse, P., Chen, J., Cheng, H.S., de Graaf, E.F., Gorczyca, J.L., Harrison, P., Hivet, G., Launay, J., Lee, W., Liu, L., Lomov, S. V., Long, A., de Luycker, E., Morestin, F., Padvoiskis, J., Peng, X.Q., Sherwood, J., Stoilova, T., Tao, X.M., Verpoest, I., Willems, A., Wiggers, J., Yu, T.X., Zhu, B.: Characterization of mechanical behavior of woven fabrics: Experimental methods and benchmark results. Compos. Part A Appl. Sci. Manuf. 39, 1037–1053 (2008). https://doi.org/10.1016/j.compositesa.2008.02.016
[32] Launay, J., Hivet, G., Duong, A. V., Boisse, P.: Experimental analysis of the influence of tensions on in plane shear behaviour of woven composite reinforcements. Compos. Sci. Technol. 68, 506–515 (2008). https://doi.org/10.1016/j.compscitech.2007.06.021